Magnetic and Mechanical 3-D Modelling of a 15 T Large Aperture Dipole Magnet

D. Martins Araujo, L. Bottura, P. Bruzzone, F. Cau, P. Ferracin, I. Pong, A. Portone, S. Prestemon, E. Ravaioli, L. Reccia, G. de Rijk, G. Sabbi, X. Sarasola and P. Testoni

***Abstract*— In 2018, two structures have been proposed with the goal of replacing the magnet EDIPO that stopped operating in 2016. These two solutions were designed to generate a field of 15 T on an aperture of 100x150 mm^2 at 4.2 K by using Nb_3Sn superconducting Rutherford cable. After the boarding review, which took place in December 2018, a solution consisting of 6-double-layers coils was retained, based on the 2-D modelling results. We now extend the study, by considering the 3-D models, with the goal of concluding the magnet conceptual design. The target is to obtain a homogeneous field, with 1% of homogeneity, over a length of 1000 mm, which allows the testing of superconducting cables for both fusion and high-energy physics. The double-layers coils, of the block-type magnet, have flared ends to allow the aperture to cross the magnet length. The 6-coils solution differs from previous similar projects as the FRESCA2 and HD2 magnets, where 4-coils were used.**

***Index Terms*—High field magnet, superconducting magnets, block-type, Nb_3Sn.**

I. Introduction

After the irreparable damage on the EDIPO magnet of the SPC (Swiss Plasma Center), in Villigen, Switzerland, due to the quench detection circuit, we aim to perform the replacement and upgrade of the magnet [1]. Inside the magnet aperture, a test well of 3-mm-thick stainless steel separates the cryogenic environment, where the samples are positioned during testing, from the helium bath cooling.

The aim of the design is to decrease the mechanical stresses in the coils in order to avoid irreversible degradation on the Nb_3Sn superconducting cable. This degradation was observed in samples tested at 4.2 K [2] under a stress of 160 MPa. As highlighted in a previous publication, the magnet has a rectangular U-shaped aperture of 100x150 mm^2 [3]. Because of that, the winding pole bends more than the poles used on accelerator magnets with round aperture usually do. The presence of magnetic forces on iron parts increases this bending, and due to this phenomenon, the stresses on coils can increase. The 6-coils solution, proposed in [4], was selected because of the lower level of peak stress, estimated in about 130 MPa by means of 2-D FEM models. Despite the increased number of coils and amount of superconducting cable, the structure has the advantage of having a low level of mechanical stresses. Section II lists the magnetic design constraints, cable and magnet parameters. The structure was modified by eliminating one of its components and by simplifying the poles shape, as shown in Section III, where the magnet geometry is described. Section IV shows the 3-D models and several results as Lorentz forces, flux density on coils and field quality. The results are compared with those obtained with the 2-D model when possible. After presenting the ANSYS 3-D mechanical model features, Section V reports the main results of the stress analysis of the magnet subjected to pre-loaded at room temperature, cooled-down to 4 K and operation at nominal field. Finally, Section VI reports some results about the quench protection of the magnet.

II. Cable, Magnet Parameters and Constraints

Table I recalls the cable parameters adopted for the magnetic modelling, which assumes the RRP® (Rod and Restack Process) 108/127 Nb_3Sn wire of 1.1 mm of diameter, as proposed for the Future Circular Collider magnets [5], is the one proposed to be used in this project. Table I also shows the parameters of the superconducting wire critical curve described on the Bottura's fitting equation [6].

Our goal is to obtain a homogeneous field of 15 T on the aperture. The length of the desired homogeneous field is 1000 mm. The maximum magnetic flux density distortion was specified to be less than 1%. An operational margin of 15% is adopted on the maximum critical current I_{ss}. These and others magnet parameters are indicated in Table II.

III. Baseline Structure

Fig. 1 shows the new baseline solution for the 15 T magnet. As indicated on Fig. 1 (a), the coils are wound around poles: a titanium pole for the inner coil and iron poles for the inter and outer coils. The flared ends block-type design can be noticed in Fig. 1 (b), where the 3-D magnet view is shown. It allows the

This work was supported by the IEEE Council on Superconductivity under contract. ABCD-123456789. *(Corresponding author: Douglas Martins Araujo.)*

This work has been carried out within the framework of the EUROfusion Consortium and has received funding from the Euratom research and training programme 2019-2020 under grant agreement No 633053. The views and opinions expressed herein do not necessarily reflect those of the European Commission.

D. Martins Araujo, L. Bottura, P. Ferracin, E. Ravaioli and G. de Rijk are with the CERN, CH-1211 Geneve, Switzerland (e-mail: douglas.martins.araujo@cern.ch).

X. Sarasola and P. Bruzzone are with the Swiss Plasma Center, École Polytechnique Fédérale de Lausanne, CH-5232 Villigen, Switzerland.

F. Cau, A. Portone, L. Reccia and P. Testoni are with the Fusion for Energy, 08019 Barcelona, Spain.

I. Pong, S. Prestemon and G. Sabbi are with the Lawrence Berkeley National Laboratory, Berkeley, CA 94720 USA.

Color versions of one or more of the figures in this paper are available online at http://ieeexplore.ieee.org.

Digital Object Identifier will be inserted here upon acceptance.

rectangular aperture to pass through the magnet; both titanium and iron poles follow this flared shape.

TABLE I
CABLE PARAMETERS AND WIRE FITTING

Parameter	Unit	Value
Wire technology	-	RRP 108/127
Wire diameter in mm	mm	1.1
Cu:non-Cu ratio	-	1.0
RRR	-	>150
Critical current density at 15 T, 4.2 K	A/mm^2	1640[a]
Critical current density at 12 T, 4.2 K	A/mm^2	3000[a]
C_0	AT/mm2	255230
$\boldsymbol{\alpha}$	-	0.96
T_{C0}	K	16
B_{C20}	T	28.8
Number of wires per cable	-	44
Bare cable width	mm	26.2
Bare cable thickness	mm	1.95
Cable insulation thickness	mm	0.15
Cable transposition	mm	155

[a] Considering 5% of degradation

TABLE II
MAGNET PARAMETERS

Parameter	Unit	Value
Aperture	mm x mm	150 x 100
Inner diameter	mm	100
Number of turns per layer (octant)		32
Operating current	kA	14.6
Bore B field	T	15.18
Peak B field in the conductor	T	15.59
Total stored magnetic energy	MJ	12.7
Operational temperature T_{op}	K	4.2
I_{op} / I_{ss} at 4.2 K	%	85

The magnet is based on the bladders and keys system [7] which, combined with an aluminum shell can provide enough pre-load to keep coils and poles in contact with an optimal distribution of contact stress. The pre-load is obtained at room temperature by filling the gap opened by the hydraulic bladders with keys, and at cold by the aluminum shell thermal contraction.

The horizontal and the vertical pads, both made of iron ensure the transferring of load from the keys and shell towards the coils. The iron yoke contributes to the magnetic shielding as well as to the structural behavior.

The bottom end part of the magnet is filled with a wedge made of stainless steel. The end plate pushes against the wedge and the end shoes, each end shoe is impregnated with the respective coil, to apply a pre-load at room temperature. At cold, the aluminum rod shrinks moving the end plate inward and increasing the axial pre-load applied to the coils. The vertical pad is mounted on the stainless steel support, which is the piece between the most outer coil and the yoke. At the end of the yoke a stainless steel plate is placed.

It can be observed that the horizontal pad is made of iron, differently from similar block-type magnets as FRESCA 2 [8]. Each double-layer coil has 64 turns (32 per layer) as the previous structure.

The coil straight section has a length of 1000 mm. The coil bending radius is at least 1000 mm, with an angle of 10º and ramp length of 200 mm, which leaves enough room to circumvent the rectangular aperture.

IV. ELECTRO-MAGNETIC MODEL AND RESULTS

Using a 2D ANSYS magnetic model, the magnet load line (electric current vs coil magnetic flux density) was produced, then the maximum current calculated with the critical curve, which after applying the 15% of margin, is 14.6 kA. With the 2D ANSYS model, we computed a magnetic flux density of 14.96 T on the aperture center.

A. Magneto Static Simulation and Forces Evaluation

Fig. 2 shows the magnetic flux density distribution on coils when feeding the magnet with 14.6 kA.

The maximum values of magnetic flux density in the coils are: 15.59 T for the inner coil, 14.41 T for the inter coil and 13.62 T for the outer coil.

In addition to the effect of the pre-load and thermal contraction on the coil stresses, the magnetic forces have to be taken into account on the mechanical analysis. These forces, both on coils and iron, play a major role on the coil stresses during nominal field operation. Table III summarizes these forces for the main components of the magnet.

TABLE III
LORENTZ AND MAGNETIC FORCES

Parameter	Fx in MN	Fy in MN	Fz in MN
Inner coil	5.42	1.01	-0.36
Inter coil	4.83	-1.60	-0.62
Outer coil	4.23	-4.99	-0.83
Iron pole (inter coil)	-2.4	-0.08	0.26
Iron pole (outer coil)	-1.68	-0.36	0.17
Vertical pad	-1.44	-1.22	0.13

The sign indicates the direction following the axis convention on Fig. 3. The forces were computed on the first quadrant

The negative vertical ($\hat{y}$) resultant force on coils is added to the magnetic forces of iron parts, which is also negative. Then, the iron poles are pushed-down and this load has to be supported by the titanium pole. Due to its rectangular shape, this load produces a bending, which changes the stress distribution on coils. Section V shows a quantitative analysis of this bending.

B. Field Homogeneity

Fig. 3 shows the magnetic field homogeneity along the aperture. The maximum magnetic flux density obtained on the center is 15.2 T, with the 3D ANSYS model. Along the x-axis, the vertical component B_y increases and reaches 15.33 T, which

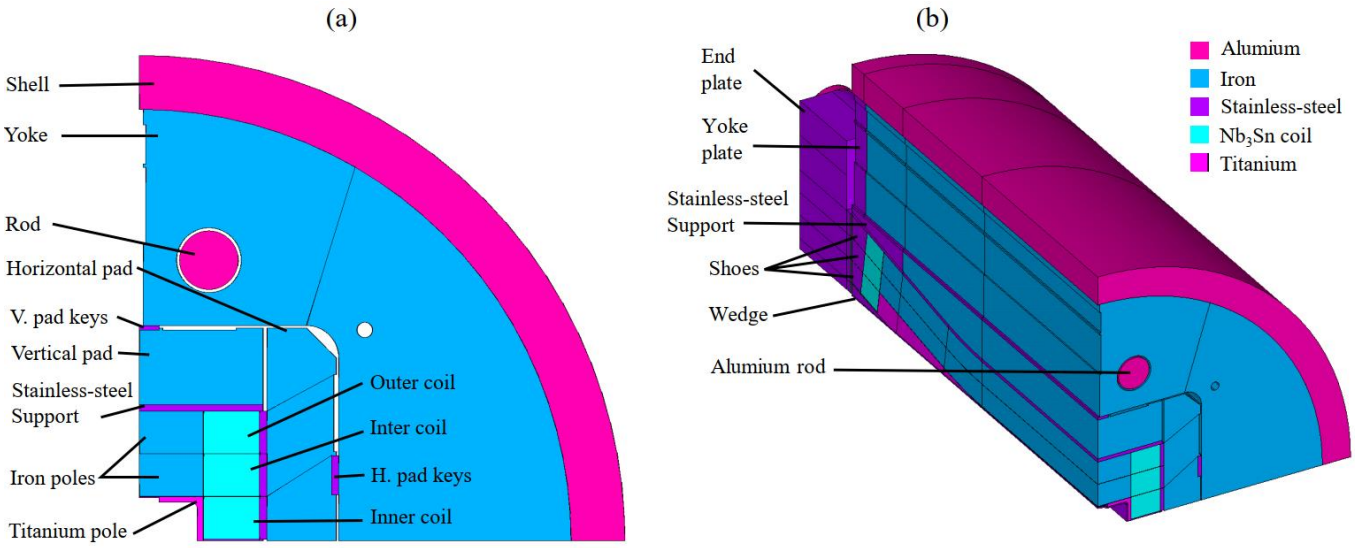

Fig. 1. (a) HEPdipo magnetic structure. The external diameter of the aluminum shell is 1260 mm. Each coil is a double-layer one, with 32 turns on each layer wound with a Rutherford type Nb_3Sn superconducting cable (b) 3-dimensional view of 1/8 of the magnet

represents 1% of distortion. The homogeneous magnetic length along the z-axis, with the criterion of 1%, is about 980 mm.

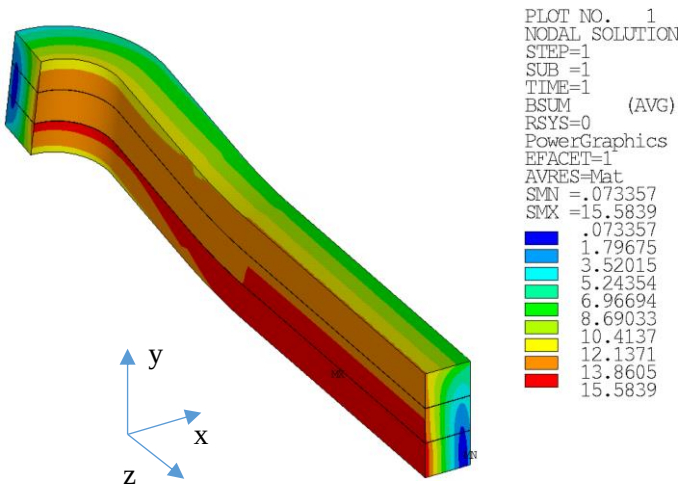

Fig. 2. Flux density on the 3-double-layer coils in T.

V. Mechanical Model and Results

The structural behavior of the magnet has been analyzed by means of a 3D FEM model developed in ANSYS. The model represents 1/8 of the entire magnet thanks to the symmetry with respect to all the three principal planes, where the boundary conditions are applied accordingly, mechanical properties are presented in Table IV.

The mesh is made of 730 thousand nodes; non-linear contacts with friction coefficient f=0.2 are provided in order to correctly represent the interactions between the components. The analysis is run as a sequence of three steps: preload at RT, cool-down and magnet energization applying magnetic forces obtained with the EM model.

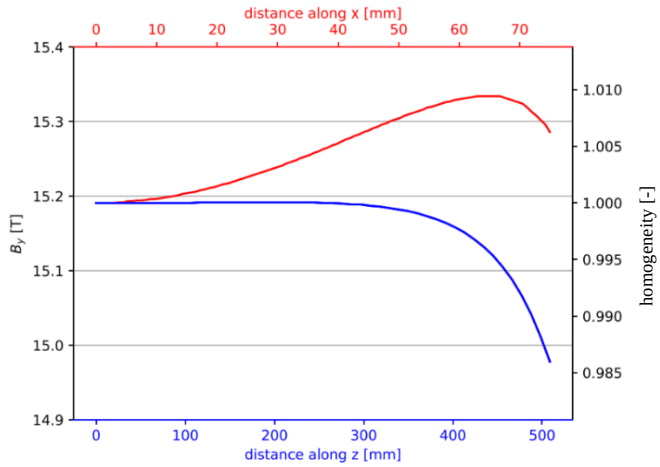

Fig. 3. Field homogeneity along the x-y plane (red curve) and along the magnet length z (blue curve)

A. Coils Stress and Titanium Pole Bending

Although the coil is a mixture of heterogeneous material, the Von Mises criterion is adopted to quantify the stress level. Fig. 4 shows the Von Mises stress when operating with 14.6 kA. Most of the coil volume is under a value of stress lower than 120 MPa, except for two peaks as indicated in Fig. 4. One peak is located at the end of the most outer coil, and it is due to the axial pre-load that has to be applied to decrease the tension between poles and coils. The other peak appears on the top of the inner coil in the straight section and increases due to the titanium pole bending, which is bonded to the inner coil. This bending is highlighted on the Fig. 5 (a) and produces a peak of stress of more than 1000 MPa as showed in the titanium pole of Fig. 5 (b). The peak of stress on the titanium pole can be managed by increasing the pole thickness and internal radius.

TABLE IV
MECHANICAL PROPERTIES

Material	Tempera-ture in *K*	Young modulus in *GPa*	Poisson's ratio	Integral thermal contraction in *mm/m*
Insulated and impregnated coils	4.3 293	25 25	0.3 0.3	3.8
Stainless steel	4.3 293	210 193	0.28 0.28	2.8
Iron	4.3 293	224 213	0.28 0.28	2.0
Aluminum	4.3 293	79 70	0.3 0.3	4.2
G10	4.3 293	30 30	0.3 0.3	7.06
Titanium	4.3 293	130 130	0.3 0.3	1.7

B. *Contacts between Coils and Poles*

Fig. 6 shows the contact pressure on the bonded contacts between coils and poles. The local pressure of more than 20 MPa on the ends of the outer coil is a consequence of the applied axial pre-load. As shown in Table V, the average tension on that part is 12 MPa for the outer coil and 48 MPa for the inter coil. If the axial pre-load is decreased, the peak of stress on the outer coil vanishes but the tension of the inter coil increases.

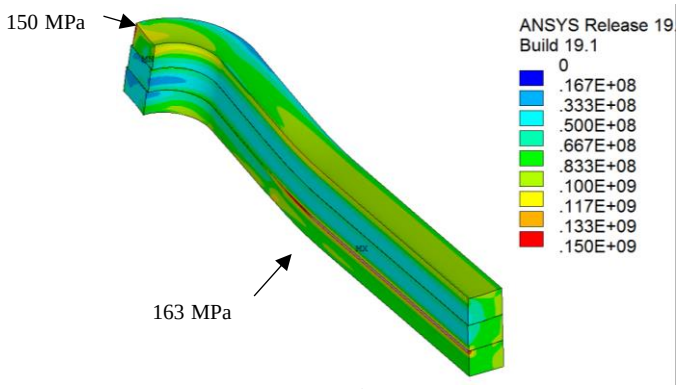

Fig. 4. Von Mises stress in Pa on coils after powering up. Color plot is limited to 150 MPa but the peak is 163 MPa. Deformation scale of 1/20.

With regard to the peak of stress of the straight section of the inner coil, which is a consequence of the titanium pole bending, on the top of the inner coil straight section, a tension of 100 MPa can be observed in Fig. 6.

C. *Stresses on Structural Parts during the 3 Steps*

Fig. 7 shows the maximum equivalent stress on coils, principal stress on iron parts and azimuthal stress on the aluminum shell.

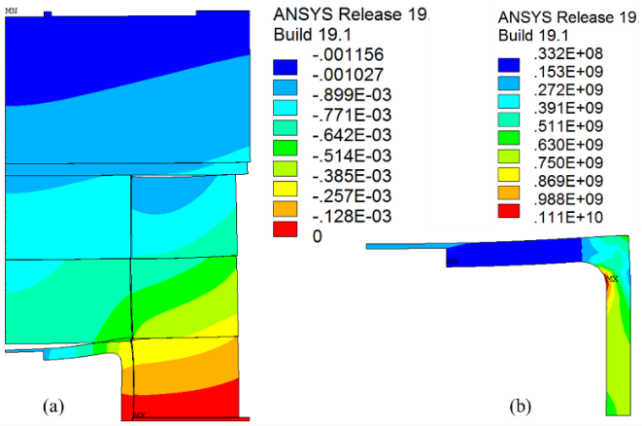

Fig. 5. Deformation scale of 1/20 (a) vertical displacement in mm on coils, poles and vertical pad (b) Von Mises stress on the titanium pole with a peak of more than 1000 MPa

TABLE V
AVERAGE CONTACT PRESSURE BETWEEN COILS AND POLES AT NOMINAL FIELD OPERATION IN MPA

Section	Inner coil	Inter coil	Outer coil
Straight	1.4	-24	-5
Hard way bend	5.4	-21	-8.5
Ramp	-2.2	-20	-15
Easy way bend	-26	-48	-12

Positive sign means compression, traction otherwise

As commented before, most of the coil volume is subjected to less than 120 MPa of Von Mises stresses except for the peaks value plotted on Fig. 5. Poles and pads undergo a maximum principal stresses of less than 280 MPa at cold, which is the stress limit to avoid damage in such brittle material [9]. The maximum hoop stress on the aluminum shell is 225 MPa.

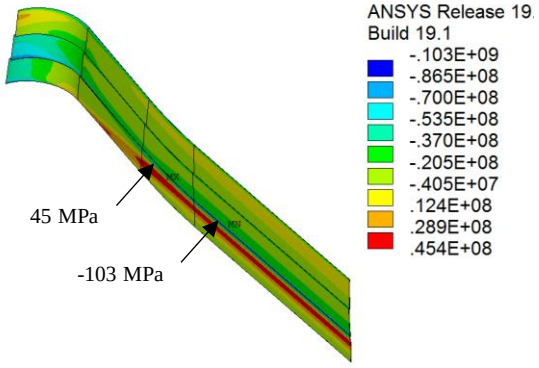

Fig. 6. Deformation scale of 1/20. Contact pressure in Pa between coils and poles at nominal field operation

VI. QUENCH PROTECTION ANALYSIS

The magnet protection in case of a quench is based on an energy-extraction (EE) system, a solution that was previously proposed for this magnet type [3]. To evaluate the performance of the protection system and design its parameters, an analysis is performed using the STEAM-LEDET program [10]. This

software allows simulating electro-magnetic and thermal transients in superconducting magnets, and includes non-linear effects such as heat exchange between turns, inter-filament and inter-strand coupling currents, and their effect on the differential inductance [11].

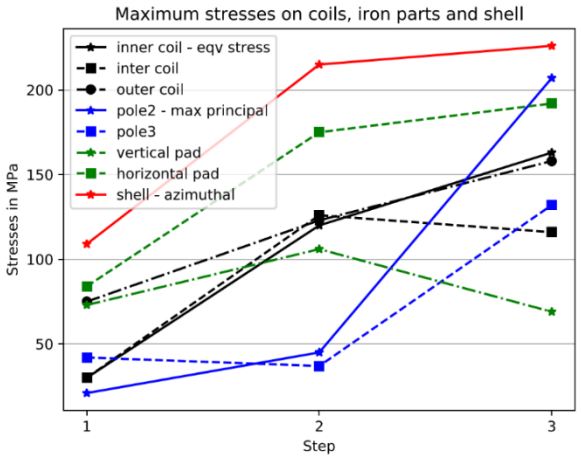

Fig. 7. Peak of stresses on the structural parts and coils for the 3 steps: 1 – pre-load; 2 – at cold; 3 – nominal field

The value of the EE resistance has a twofold effect on the quench protection performance. On the one hand, increasing the EE resistance allows extracting the magnet stored energy more quickly, and hence reducing the hot-spot temperature after a quench. On the other hand, the peak voltage across the EE resistor, and hence the peak voltage to ground, depend linearly on the EE resistance. Thus, the EE resistance is selected as a compromise between the conflicting needs of minimizing hot-spot temperature and voltage to ground. The simulated hot-spot temperature versus peak voltage across the EE resistor, for values of constant EE resistance between 35 and 141 mΩ, is plotted in Fig. 8 as well as the EE voltage, which can be half of the indicated value if symmetric grounding is adopted.

The simulated magnet current and hot-spot temperature, which has a maximum of 209 K after a quench at nominal current, for the selected constant EE resistance of 106 mΩ, are shown in Fig. 9. The presence of inter-filament coupling currents, which reduce the magnet differential inductance and generate local loss, hence causing quench back, affects significantly the transient causing a faster magnet discharge. This result can be observed in Fig. 9, where the magnet current in the case of a purely exponential discharge is also plotted.

VII. Summary

After the preliminary design study of a 15 T large aperture magnet for cable and insert testing, two structures were retained as candidates for the EDIPO magnet replacement. A decision was taken in favor of the 6 double-layer coils, all of them with the same number of turns.

The conceptual design has been investigated by means of 3-D electro-magnetic and mechanical FEM models. The results of the EM analysis show that the targets of magnetic field value (15 T) and uniformity in the straight section (980 mm) are met. With regard to mechanical behavior, the stress level seems acceptable in all the components and for the majority of the coil volume. Some local peaks will be addressed in the following steps of the design optimization.

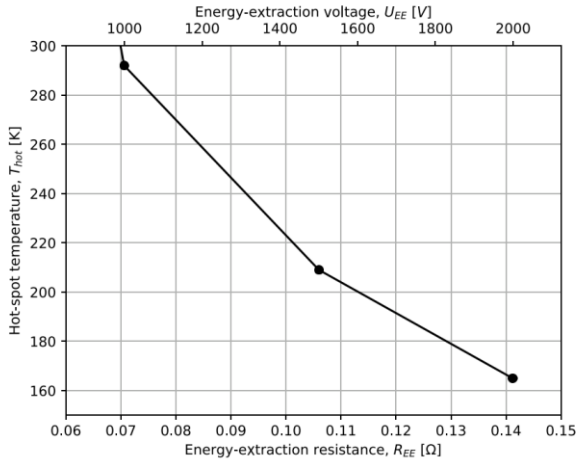

Fig. 8. Hot-spot temperature for the energy extraction protection for different values of resistance and voltage.

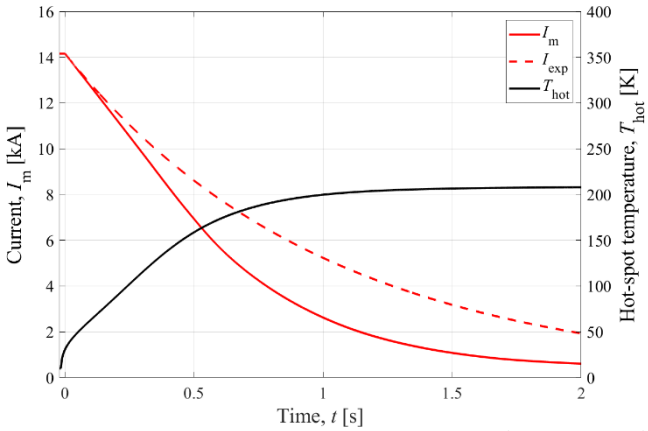

Fig. 9 Simulated magnet current and hot-spot temperature for a voltage of 1.5 kV.

References

[1] P. Bruzzone, B. Stepanov, D. Uglietti, R. Wesche, and K. Sedlak, 'EDIPO: The Test Facility for High-Current High-Field HTS Superconductors', *IEEE Trans. Appl. Supercond.*, vol. 26, no. 2, pp. 35–40, Mar. 2016.

[2] J. Duvauchelle, B. Bordini, J. Fleiter, and A. Ballarino, 'Critical Current Measurements Under Transverse Pressure of a Nb3Sn Rutherford Cable Based on 1 mm RRP Wires', *IEEE Trans. Appl. Supercond.*, vol. 28, no. 4, pp. 1–5, Jun. 2018.

[3] P. Bruzzone *et al.*, 'Conceptual Design of a Large Aperture Dipole for Testing of Cables and Insert Coils at High Field', *IEEE Trans. Appl. Supercond.*, vol. 28, no. 3, pp. 1–5, Apr. 2018.

[4] X. Sarasola *et al.*, 'Magnetic and Mechanical Design of a 15-T Large Aperture Dipole Magnet for Cable Testing', *IEEE Trans. Appl. Supercond.*, vol. 29, no. 5, pp. 1–5, Aug. 2019.

[5] D. Tommasini *et al.*, 'The 16 T Dipole Development Program for FCC', *IEEE Trans. Appl. Supercond.*, vol. 27, no. 4, pp. 1–5, Jun. 2017.

[6] L. Bottura and B. Bordini, 'Jc(B,T,ε) Parameterization for the ITER Nb3Sn Production', IEEE Trans. Appl. Supercond., vol. 19, no. 3, pp. 1521–1524, Jun. 2009.

[7] S. Caspi et al., 'The use of pressurized bladders for stress control of superconducting magnets', IEEE Trans. Appl. Supercond., vol. 11, no. 1, pp. 2272–2275, Mar. 2001.

[8] G. Willering et al., ‘Cold Powering Tests and Protection Studies of the FRESCA2 100 mm Bore Nb3Sn Block-Coil Magnet’, IEEE Trans. Appl. Supercond., vol. 28, no. 3, pp. 1–5, Apr. 2018.
[9] A. Portone et al., ‘Design and optimization of the 12.5T EFDA dipole magnet’, Cryogenics, vol. 46, no. 7, pp. 494–506, Jul. 2006.
[10] ‘STEAM: Simulation of Transient Effects in Accelerator Magnets - Home’. [Online]. Available: https://espace.cern.ch/steam. [Accessed: 17-Sep-2019].
[11] E. Ravaioli et al., ‘Modeling of Interfilament Coupling Currents and Their Effect on Magnet Quench Protection’, IEEE Trans. Appl. Supercond., vol. 27, no. 4, pp. 1–8, Jun. 2017.